Order-disorder phase transitions of oxygen on Rh(100)

A. Baraldi, V. R. Dhanak,* G. Comelli,† K. C. Prince, and R. Rosei†
Sincrotrone Trieste SCpA, Padriciano 99, I-34012 Trieste, Italy
(Received 30 July 1996; revised manuscript received 21 February 1997)

The adsorption and ordering of oxygen atoms on the Rh(100) surface have been investigated by spot profile low-energy electron diffraction measurements as a function of coverage and temperature. Three oxygen induced structures were observed: $p(2\times2)$, $c(2\times2)$, and $(2\times2)p4g$. Using the intensity and the full width at half maximum of the diffraction spots, the $(2\times2)p4g\rightarrow c(2\times2)$ and $c(2\times2)\rightarrow(1\times1)$ order-disorder phase transitions have been characterized and the phase diagram mapped out. The $(2\times2)p4g\rightarrow c(2\times2)$ transition is assigned to the two-dimensional Ising universality. The role of the adsorbate-adsorbate interactions in the formation of the ordered phases and the kind of defects involved in the order-disorder phase transitions are discussed. [S0163-1829(97)06935-X]

I. INTRODUCTION

When atoms or molecules adsorb on a surface, they interact not only with the substrate but with each other as well. A noninteracting lattice gas would always give rise to a $p(1\times1)$ structure only, whereas, adsorbate-adsorbate interactions can cause the formation of other ordered structures. The symmetry of these superstructures is determined by the qualitative nature of the interactions. For chemisorbed systems, lateral interactions between adsorbed atoms or molecules, due to long-range dipole-dipole interactions or indirect electronic interactions, are generally an order-of-magnitude weaker than the adsorbate-surface interaction, particularly at low coverage. In this surface coverage range, the influence of lateral interactions on the energy of the layer is of minor importance, but the statistical distribution of the adsorbates in space deviates from the behavior of a noninteracting system.[1] The factors which govern the lattice-gas system have important consequences for the kinetics of adsorption and desorption, ordering processes, order-disorder phase transitions, and chemical reactions on surfaces.

The system O/Rh(100) is a good candidate for investigation of these phenomena. It is known from previous studies[1–9] that at room temperature on the (100) rhodium surface oxygen forms three different ordered structures: a $p(2\times2)$ at 0.25 ML, an intermediate $c(2\times2)$, and a $(2\times2)p4g$ at saturation (0.5 ML). For all structures, oxygen sits in the fourfold hollow site position; in the $p4g$ structure, the substrate additionally reconstructs by rotation of the four Rh atoms nearest to each oxygen atom.

In this paper, we report measurements of low-energy electron diffraction (LEED) superlattice spot intensities and spot profiles in the whole oxygen coverage range. The absence of a (1×1) structure at high oxygen coverage implies that the lateral nearest-neighbor interactions are strongly repulsive, limiting the saturation coverage to 0.5 ML. The $(2\times2)p4g$ structure, consisting of a $c(2\times2)$ arrangement of oxygen atoms on a reconstructed substrate, requires a short-range next-nearest-neighbor repulsive interaction in addition to the attraction required for $p(2\times2)$ island formation at low coverage.

We observe two phenomena: a $p(2\times2)\rightarrow c(2\times2)$ transition, interpreted previously[5] as an Ising-like order-disorder phase transition with $T_c=450$ K, as well as a series of $(2\times2)p4g\rightarrow c(2\times2)$ and $c(2\times2)\rightarrow(1\times1)$ transitions at temperatures which are coverage dependent. The analysis of the critical exponents shows that the $(2\times2)p4g\rightarrow c(2\times2)$ transition belongs to the two-dimensional (2D) Ising universality class.

Only a few phase diagram studies of oxygen on metal surfaces have been reported previously, for example, O/W(110),[10] O/Ni(111),[11] O/Ni(100),[12,13] and O/Ru(001).[14]

In the next section we describe the experimental techniques used, and in Secs. III A and III B we present the results of constant temperature and constant coverage spot profile measurements, respectively. In the last section the results are discussed.

II. EXPERIMENT

The experiments were carried out in a mu-metal UHV chamber (base pressure of 1×10^{-10} mbar), equipped with a spot profile analysis (SPA)-LEED system (Omicron GmbH) which has an instrumental transfer width larger than 750 Å at an electron-beam energy of 115 eV.[15] The Rh crystal was cut and mechanically polished to within 0.5° of the (100) direction. Initially, it was prepared in the UHV chamber by many cycles of 2 keV Ar^+ bombardment, annealing to 1170 K and oxygen treatment at 970 K to remove residual carbon. After this cleaning procedure, the LEED spots from the Rh surface were symmetric and had a full width at half maximum (FWHM) under antiphase conditions of ~0.005 Å^{-1}, which indicates that the average terrace width on the surface was at least 500 Å. Previous scanning tunnel microscope (STM) measurements[6] on the same sample also showed large flat terraces and we can conclude that the sample contained a negligible density of defects like steps, which introduce a displacement along the normal to the surface.

Before oxygen exposure, the Rh sample was flashed to 600 K to remove any CO or H adsorbed from the background. Spot profile measurements of the oxygen-induced half order diffraction beams were performed in two different ways: (i) at constant temperature while dosing oxygen at a

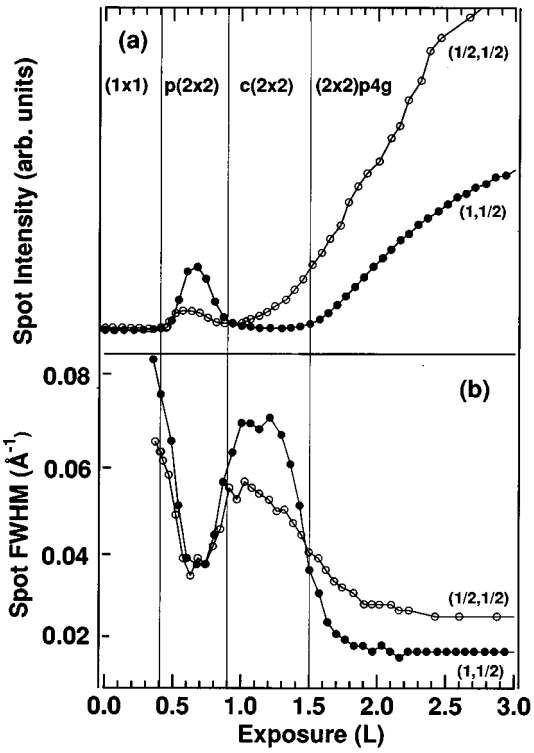

FIG. 1. Intensity (a) and FWHM (b) vs dose (Langmuir) for the $(1,\frac{1}{2})$ (filled circles) and the $(\frac{1}{2},\frac{1}{2})$ (open circles) spots obtained dosing oxygen at a pressure of 5×10^{-9} mbar and at $T=400$ K.

pressure of 5×10^{-9} mbar; (ii) at constant oxygen coverage while raising the temperature.

For the first case the sample temperature was kept constant to within ±1 K. In the second case, to compensate for the loss of adsorbed oxygen due to reaction with hydrogen or CO from the ambient, a partial pressure of oxygen in the 10^{-10} mbar range was maintained during the experiments, so that the intensity and FWHM of the $(1,\frac{1}{2})$ and $(\frac{1}{2},\frac{1}{2})$ spots after repeated heating/cooling cycles was reproducible. The SPA-LEED was operated at 58 eV electron-beam energy, which corresponds roughly to maxima of the $(1,\frac{1}{2})$ and $(\frac{1}{2},\frac{1}{2})$ spot intensities.

III. RESULTS

A. Constant-temperature measurements

Figure 1(a) compares the intensity variations of the $(1,\frac{1}{2})$ and $(\frac{1}{2},\frac{1}{2})$ beams (filled and empty circles, respectively) as a function of the oxygen exposure. Four regions can be distinguished, corresponding to different ordering of the overlayers: (i) (1×1), where neither extra spots are visible; (ii) $p(2\times2)$, with both spots showing an intensity with a maximum around 0.65 L ($1\,\mathrm{L}=1.33\times10^{-6}$ mbar s); (iii) $c(2\times2)$, where only the $(\frac{1}{2},\frac{1}{2})$ spot is present; (iv) $(2\times2)p4g$ where both spots display a continuous intensity increase.

The FWHM of the diffraction spots, shown in Fig. 1(b) is reduced at the maxima of the spot intensity for the $p(2\times2)$ and $(2\times2)p4g$ structures, indicating good ordering.

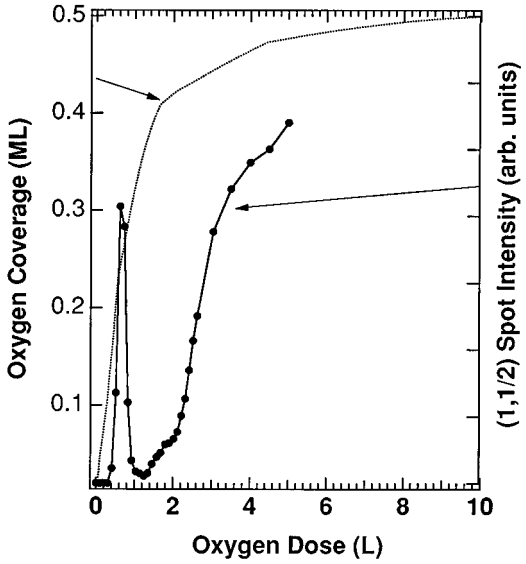

FIG. 2. O 1s photoemission intensity (dotted curve) and $(1,\frac{1}{2})$ spot intensity (filled curve) vs dose (Langmuir). Oxygen pressure: 5×10^{-9} mbar; $T=370$ K.

In order to calibrate the oxygen coverage, we used previous x-ray photoemission spectroscopy (XPS) measurements of the oxygen uptake, performed in another chamber but with the same sample. The XPS uptake data are shown in Fig. 2 together with the $(1,\frac{1}{2})$ spot intensity. Assuming that the maximum intensity of the $p(2\times2)$ half-order spots corresponds to 0.25 ML, the coverage was calibrated up to saturation.

This calibration allowed us to plot in Figs. 3 and 4, respectively, the intensities of the $(1,\frac{1}{2})$ and $(\frac{1}{2},\frac{1}{2})$ spots, $I_{1,1/2}(\Theta)$ and $I_{1/2,1/2}(\Theta)$, as a function of the oxygen coverage for different temperatures, ranging from 325 to 800 K. The intensities have not been corrected for the Debye-Waller factor because its value is strongly dependent on surface structure and coverage. Two distinct regions can be distinguished in the spectra: (i) from 0 to 0.35 ML and (ii) from 0.35 ML to saturation.

For temperatures below 450 K, both spots grow in intensity above 0.15 ML, reach a maximum at 0.25 ML, and then decrease from 0.25 to 0.35 ML. This is associated with the formation of the $p(2\times2)$ ordered phase. At slightly higher temperatures, the $(1,\frac{1}{2})$ spot disappears while the $(\frac{1}{2},\frac{1}{2})$ spot is still present though reduced in intensity. These results are consistent with the existence of the $p(2\times2)\rightarrow c(2\times2)$ order-disorder phase transition described in our previous work.[5] The high-temperature phase is disordered in the sense that order is reduced because the order parameter corresponding to the $(1,\frac{1}{2})$ diffraction spots has vanished but the $(\frac{1}{2},\frac{1}{2})$ order parameter is nonzero. In real space, this implies that the oxygen atoms are disordered with respect to a $p(2\times2)$ lattice. We return to this point below in the discussion of defects and surface Burgers vectors.

At very high temperature, but still below the oxygen desorption temperature of 840 K, the $(\frac{1}{2},\frac{1}{2})$ spot almost vanishes.

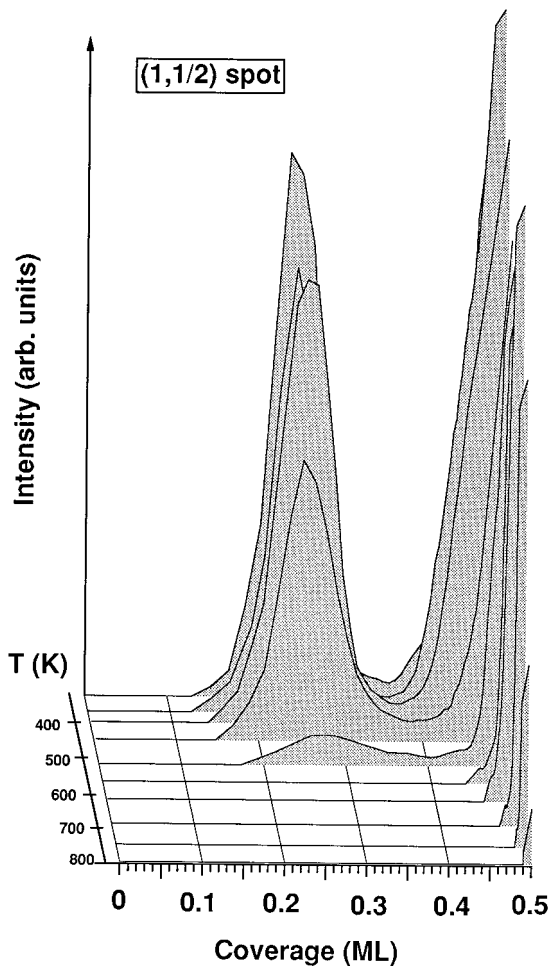

FIG. 3. Intensity of the $(1,\frac{1}{2})$ spot as a function of oxygen coverage at different substrate temperatures.

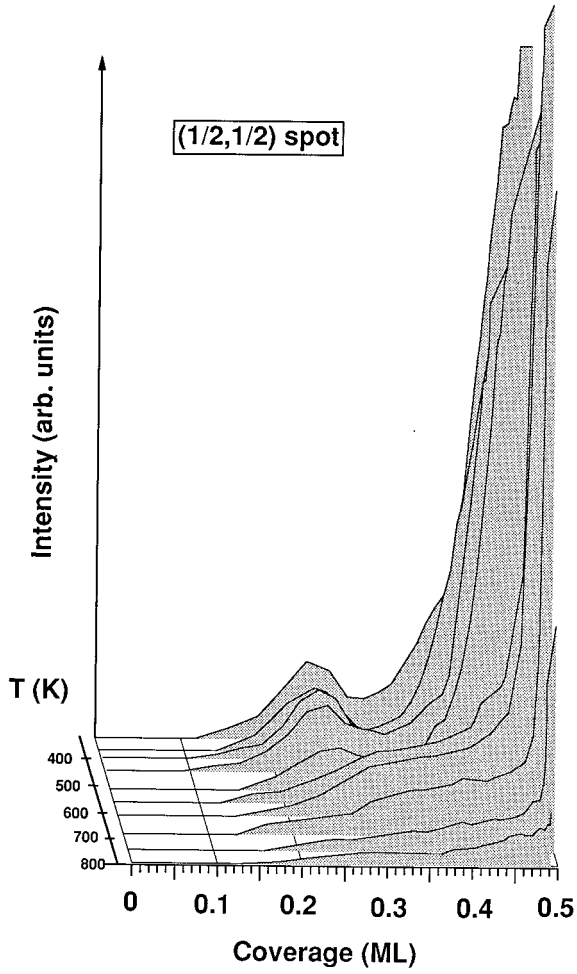

FIG. 4. Intensity of the $(\frac{1}{2},\frac{1}{2})$ spot as a function of oxygen coverage at different substrate temperatures.

Above 0.35 ML both spots grow in intensity for increasing oxygen coverages at all temperatures. Two features should be noted: (i) as the coverage approaches 0.5 ML, a sharp increase in intensity of both spots occurs; (ii) comparing intensities relative to coverage for different temperatures, a sharp decrease with increasing temperature is visible.

These data allow us to draw the qualitative phase diagram represented in Fig. 5. In principle, phase diagrams should be determined by measuring the intensity versus temperature curves at various constant coverages using the temperature of the respective inflection points as transition temperatures and phase boundaries. Since the absolute coverage cannot be determined in our SPA-LEED system, we have used the photoemission data as described above and have assumed that the sticking coefficient is independent of temperature in determining the coverage used for the phase diagram.

B. Constant coverage measurements

As shown previously[5] the stoichiometric $p(2\times2)$ ordered structure undergoes an order-disorder phase transition at a critical temperature T_c of 450 ± 5 K. The $p(2\times2)\rightarrow c(2\times2)$ transition was found to be second order and belongs to the 2D-Ising universality class. In this section we concentrate our attention on the temperature dependence of the $(2\times2)p4g$ phase.

An order-disorder phase transition also occurs for the $(2\times2)p4g$ structure as seen by the variation with temperature of the fractional order spots' intensity. Some data for the $(1,\frac{1}{2})$ spot are presented in Fig. 6. The spot intensity has been corrected for the Debye-Waller factor by measuring and removing the temperature dependence of the intensity at low temperature. The thermal diffuse background was subtracted.

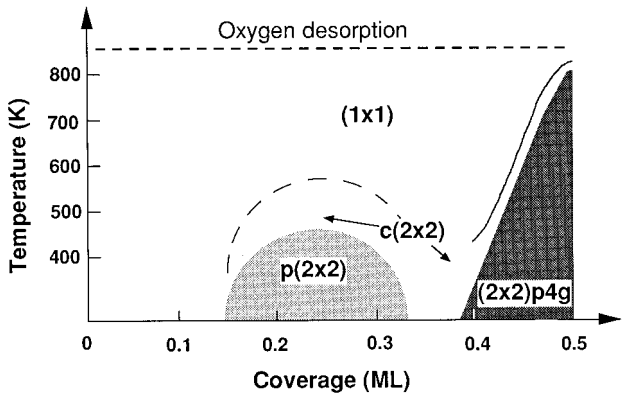

FIG. 5. Phase diagram sketch. The continuous line defines the border between $c(2\times2)$ and (1×1) phase; the dashed line a possible separation.

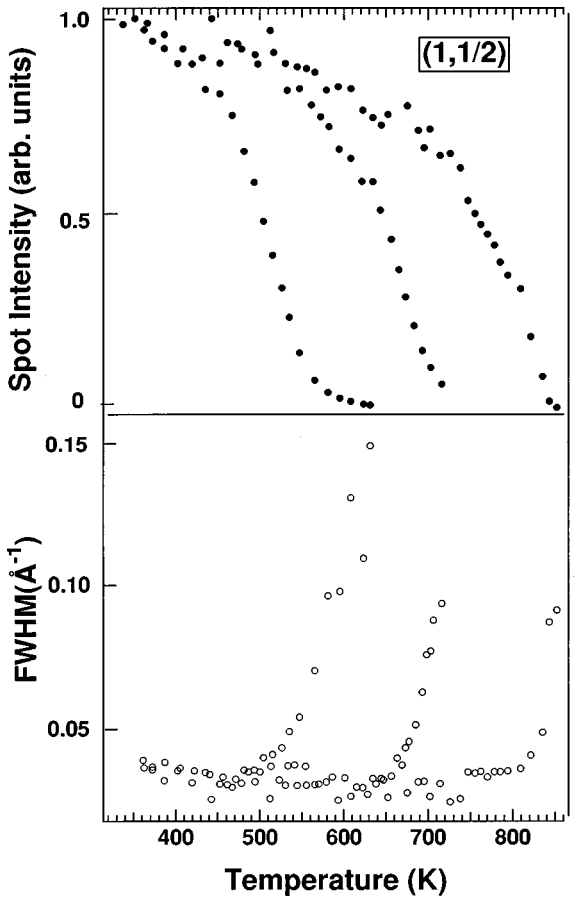

FIG. 6. Normalized peak intensity and FWHM vs temperature of the $(1,\frac{1}{2})$ diffraction spot for the $(2\times2)p4g$ at different oxygen coverages between 0.42 and 0.5 ML. Solid circles, measured peak intensity corrected by the Debye-Waller factor; open circles, measured FWHM.

The point of inflection of the intensity curves, shown in Fig. 6(a), coincides approximately with the onset of spot broadening in Fig. 6(b) and is identified with the temperature T_c of the order-disorder phase transition. Data shown refer to $(2\times2)p4g$ layers with different oxygen coverages ranging from 0.42 to 0.5 ML. Higher oxygen doses correspond to higher transition temperatures. The effect of disorder due to nonstoichiometry is thus to reduce the transition temperature.

The continuous change of the intensity across the transition is indicative of second-order behavior. The critical exponents were extracted by fitting the data to appropriate expressions, for example,

$$I\sim|(T-T_c)/T_c|^{2\beta},\quad T<T_c\,.$$

The exponent β is associated with the long-range-order parameter. Above T_c intensity persists due to scattering from critical fluctuations, i.e., short-range order. The exponent γ associated with the susceptibility was extracted using the expression

$$I\sim|(T-T_c)/T_c|^{-\gamma},\quad T>T_c\,.$$

Finally, the temperature dependence of the FWHM above T_c reflects the critical behavior of the correlation length ν through the expression

TABLE I. Measured and calculated critical exponents for the nonstoichiometric $(2\times2)p4g\rightarrow c(2\times2)$ phase transition. ''calc.'' indicates values derived from the experimentally determined exponents.

Exponent	T_c temperature range[a] (K)	Measured value	Theoretical Ising value
ν	510–560	1.07 ±0.24	1
	600–660	0.98 ±0.28	
β	500–550	0.121±0.010	0.125
	600–660	0.123±0.011	
γ	500–550	1.67 ±0.28	1.75
	600–660	1.70 ±0.56	
α (calc.)	510–550	−0.14 ±0.48	0
		0.08 ±0.28	
	600–660	0.04 ±0.56	
η (calc.)	510–550	0.23 ±0.05	0.25
	600–660	0.25 ±0.07	

[a]Since T_c varies with the oxygen coverage, we have grouped the results according to T_c value.

$$\mathrm{FWHM}\sim|(T_c-T)/T_c|^{\nu},\quad T>T_c\,.$$

We first calculated T_c and the exponent ν from the FWHM temperature dependence; depending on the oxygen coverage, T_c varies from 510 to 810 K. The latter value is very close to the oxygen desorption temperature (840 K). The other exponents were then extracted from the intensity data and are summarized in Table I. T_c values extracted from the width analysis are in agreement with the values obtained from the intensity data within the average error of ±8 K.

The results allow us to exclude the four-state Potts model universality class, for instance, as the values of ν, β, and α are inconsistent. Within the error bars, the exponents are consistent with either the Ising class or the three-state Potts class for all temperatures below 660 K. The three-state Potts model is inappropriate as it requires three values of the spin (within the language of statistical magnetic models), while in our case only two are available due to the fourfold symmetry of the surface. We therefore conclude that the $(2\times2)p4g\rightarrow c(2\times2)$ transitions belong to the Ising class at all coverages.

The $(\frac{1}{2},\frac{1}{2})$ curves (not shown) reach the inflection point at temperatures which are always about 20 K higher than the corresponding $(1,\frac{1}{2})$ spot temperature, measured from the same layer. This is in agreement with the measurements at constant temperature, plotted in Figs. 3 and 4, where the $(\frac{1}{2},\frac{1}{2})$ spot appeared at higher temperatures than the $(1,\frac{1}{2})$ spot. For this reason we believe that there are two order-disorder phase transitions: $(2\times2)p4g\rightarrow c(2\times2)$ and a successive $c(2\times2)\rightarrow(1\times1)$, occurring about 20 K higher in temperature.

Only the data at relatively low coverage have been considered in the evaluation of the critical exponents. The data analysis at $T_c>720$ K is strongly influenced by the stoichiometry of the system. Figure 6(a) clearly shows that even at this temperature, the $p4g$ structure undergoes a phase transition, but we cannot exclude a possible loss of some oxygen

because we are very close to the desorption temperature. At $T>720$ K we obtained values for the β parameter ranging from 0.14 to 0.16, i.e., a little higher than the Ising value of 0.125. However, the critical exponents ν and γ extracted from the measurements are consistent with those expected for the 2D Ising universality class at these coverages.

Landau theory predicts that only two exponents are independent while the others can be determined from the universal scaling relations:

$$d\nu=2-\alpha,$$

$$\alpha+2\beta+\gamma=2,$$

$$\eta=2\beta/\nu,$$

where $d=2$ for surfaces.

The theoretical value of the critical exponent α associated with the specific heat change at the phase transition is zero, and we can evaluate it from the data using either of the first two equations, since we have measured γ, β, and ν independently. The exponent η associated with the correlation function can be calculated from the third equation and is consistent with the Ising class. The values of the critical exponents obtained from this analysis are shown in Table I, and are in agreement with the theory for an Ising transition, although the error bars are fairly large for α.

An independent measure of α can be obtained from the integrated intensity of the half-order spots, which follows the equation:

$$I(t)=A_0+A_1t\pm B_{-+}|t|^{1-\alpha}+\cdots,$$

where

$$t=|T-T_c|/T_c.$$

This approach is valid only when the range of integration over k is large enough and the temperature range is close enough to T_c. The critical exponent α determined by fitting the expression is 0.02 ± 0.04 in the whole coverage range of the $(2\times2)p4g$ structure, in close agreement with the value for the Ising universality class.

A final point worth considering is the effect of imperfections of the substrate and defects. These finite-size effects smear out the phase transition in temperature and leave an intensity tail above an average T_c. The fluctuation correlation length L_c increases as $T\rightarrow T_c$ according to the expression[16,17]

$$L_c\sim a[|T-T_c|/T_c]^{-\nu},$$

where a is the lattice constant. The theory predicts that only for domain size greater than L_c, as in our case, is the expression valid. L_c is ~200 Å, a is 2.69 Å, and T_c is between 500 and 850 K. The shift in measured critical temperature due to these defects is

$$\Delta T=AL_c^{-\nu}T_c,$$

where the constant A is about 1.25. Thus finite-size effects could cause a downward shift of the measured T_c by about 3–5 K, which is within the range of the experimental error.

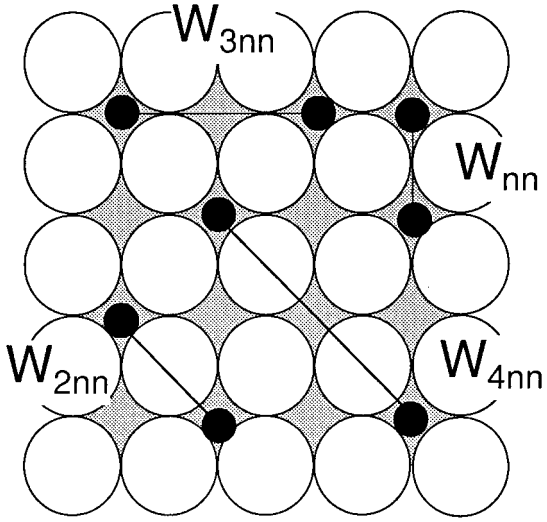

FIG. 7. Adsorbate-adsorbate oxygen interactions. W_{nn}, W_{2nn}, etc. refer to the nearest-neighbor, second-nearest-neighbor, etc. interaction energies. Lines indicate the interaction distance.

IV. DISCUSSION

We first consider the nature and range of the oxygen-oxygen interactions. These interactions can be mediated via the metallic substrate over a distance of up to several lattice constants. The experimental evidence for adlayer ordering well below a half-monolayer coverage indicates that long-range interactions among the adsorbed oxygen atoms exist, at least over distances corresponding to third-nearest neighbors.

In the experimentally measured $I_{1,1/2}(\Theta)$ and $I_{1/2,1/2}(\Theta)$ curves, Figs. 3 and 4, the fractional-order beam intensities become so weak at coverages below 0.15 ML that both the beam sharpness and the $I(\Theta)$ curve are difficult to evaluate. This implies that the tendency for island formation is not strong, and so the interaction energy with the fourth-nearest neighbor, W_{4nn}, Fig. 7, and longer distances, is less than the thermal energy K_BT. At low coverage (<0.15 ML) the O adatoms can be almost randomly distributed over the surface, in one of the four equivalent sublattices that exist for the $p(2\times2)$ structure, in a sea of disordered lattice gas of low density.

As the coverage increases above 0.15 ML, the quadratic form of the $(1,\frac{1}{2})$ spot intensity curve in Fig. 3 indicates that island growth is occurring. As noted above, the tendency is not strong, indicating that the attractive interaction W_{3nn} is weak. Comparison between this experiment and adsorption performed at lower temperature (150 K) indicates that the process of ordering of the $p(2\times2)$ structure is not significantly affected by the temperature, so the transitions observed are in equilibrium and not kinetically limited.

At coverage greater than 0.25 ML there are two possible mechanisms for the $p(2\times2)$ to evolve into the $c(2\times2)$ structure. Oxygen atoms could be added at random sites to form nuclei for domains of $c(2\times2)$ without disturbing the coherence of the surrounding $p(2\times2)$ structure. In this case the nuclei are pointlike. Alternatively, the additional atoms can form extended structures that are locally $c(2\times2)$ and that break the translational symmetry of surrounding

$p(2\times2)$ domains. This would imply diffusion of one domain with respect to the other.

The nonlinear decrease in the fractional-order LEED beam intensity with coverage for $\Theta > 0.25$ ML, evident in Figs. 3 and 4, favors the second mechanism. Random adsorption of extra atoms on $c(2\times2)$ sites in the $p(2\times2)$ units cell would give only a linear decrease in the spot intensity. The broadening of the FWHM of the $(1,\frac{1}{2})$ diffraction spot, which is characteristic of the $p(2\times2)$ structure, is also consistent with symmetry breaking. The evidence therefore points to the formation of extended defects as the first step in the formation of the $c(2\times2)$ structure.

The transition $p(2\times2)\rightarrow c(2\times2)$ at constant temperature and varying coverage thus appears to be a continuous, i.e., second order, transition mediated by heavy domain walls. Over most of its existence range, the $c(2\times2)$ phase is nonstoichiometric and partly disordered.

From the point of view of interaction energies, the formation of the $c(2\times2)$ after the $p(2\times2)$ structure indicates that $W_{2\mathrm{nn}}$ is repulsive.

The $c(2\times2)$ in principle has a local coverage of 0.5 ML, but before reaching this coverage the structure transforms to $(2\times2)p4g$. Thus the $c(2\times2)$ is always nonstoichiometric. As seen in Fig. 3 the $(1,\frac{1}{2})$ spot, characteristic of the final $(2\times2)p4g$ geometry, starts to grow below 0.5 ML. This means that extra atoms locally induce the substrate reconstruction, while other parts of the surface are still covered by $c(2\times2)$ in small islands. It should be noted by comparison with the XPS uptake curve in Fig. 2, that the final region of ordering occurs over a wide range of exposures very close to the saturation coverage of oxygen. This implies that a significant cooperative ordering effect takes place in the final stage of chemisorption, i.e., above 0.42 ML, which is induced by the addition of a small number of oxygen adatoms to a nearly saturated oxygen overlayer at this temperature.

The $(2\times2)p4g$ structure has islands at least 200 Å wide, larger than for the $p(2\times2)$, which are $\sim$150 Å. This provides further evidence for the good substrate quality. Only a small percentage of defects (like steps, vacancies, contaminants, etc.) is sufficient to break the long-range order.[18]

Some phase diagrams show asymmetry around a stoichiometric coverage, i.e., 0.25 ML for the $p(2\times2)$ phase, and theoretical studies have concluded that many-body interactions are of fundamental importance to describe this asymmetry.[19] In our case, the symmetry of the $p(2\times2)$ phase around 0.25 ML indicates that the approximation of the lattice-gas model in this range of coverages is adequate. This means that the Ising spin model with pairwise interactions is a sufficiently good approximation for the present system at coverages <0.35 ML.

The interpretation of the mutual O-O interaction at high coverage is more difficult. A lattice-gas description is inappropriate for a substrate that reconstructs in the presence of the overlayer. For the $(2\times2)p4g$ case we should in fact consider the contribution arising from the elastic distortions of the substrate and the consequent changes in the electronic properties of the surface. While the $p(2\times2)$ structure is symmetric with respect to coverage, we cannot determine whether the $p4g$ structure is so because continued dosing does not increase the coverage. This is attributed to strong repulsive interactions for oxygen atoms on adjacent sites which forbids adsorption. The influence of repulsive interaction between neighboring adsorbates is also confirmed by the low-temperature shoulder in thermal-desorption spectra obtained by Salanov and Savchenko.[20]

One question which arises is why oxygen induces a $p4g$ structure on Rh, but not on neighboring metals such as Ni, Cu, and Pd. For the analogous reconstruction induced by N and C on Ni(100) Reindl, Aligia, and Bennemann[21] concluded that for atomic radii larger than a critical value, no substrate reconstruction occurs. On Ni(100), N and C induce a $p4g$ structure, but O which is larger does not. In our case the Rh-Rh distance (2.78 Å) is greater than the Ni-Ni distance (2.49 Å) and the critical radius in this case would be bigger and greater than the oxygen covalent radius.

As noted above, both the $(2\times2)p4g\rightarrow c(2\times2)$ and the $p(2\times2)\rightarrow c(2\times2)$ transitions appear to belong to the Ising universality class. Disordering at the critical temperature is then described in terms of the vanishing of the free energy of formation for a particular type of defect, which therefore proliferates. In our previous work, we described the defects associated with the $p(2\times2)\rightarrow c(2\times2)$ transition as domain walls of surface Burgers vector $\mathbf{b}=a'(110)$, where a' is the surface lattice parameter. The microscopic model of this transition is of an ordered, $p(2\times2)$ structure of coverage 0.25, at low temperature with oxygen atoms located in the fourfold hollow sites. Just above the critical temperature the $c(2\times2)$ structure has the same coverage and short-range order exists, but the long-range (2×2) order parameter [corresponding to the $(1,\frac{1}{2})$ spots] has vanished.

Similarly, the $(2\times2)p4g$ structure transforms to $c(2\times2)$ by the creation of defects and just above its critical temperature consists of short-range $p4g$ ordered regions separated by defects. The oxygen atoms remain on fourfold hollow sites and are ordered with respect to one another. The long-range ordering of the Rh atoms in their rotated positions disappears.

For the $c(2\times2)\rightarrow(1\times1)$ transition we were not able to determine the universality class because the critical temperature is too close to the desorption temperature. If we assume that it is also Ising-like, the only possible defects are those with Burgers vector $\mathbf{b}=a'(100)$ and $a'(100)$ illustrated in Fig. 8. The defect is either stoichiometric (negative Burgers vector) or has a locally lower concentration of oxygen (positive Burgers vector). This immediately provides insight into why the $c(2\times2)$ with coverage <0.5 can disorder: it does so by the formation of the second kind of defect. At $\Theta=0.5$, the $c(2\times2)$ structure can transform to a (1×1) only by means of defects of the type $a'(100)$. These require oxygen atoms on strongly repulsive, nearest-neighbor sites.

The effect of nonstoichiometry on the critical exponents can be discussed within the framework of Fisher renormalization theory.[22] The variation of concentration from 0.5 can be regarded as a ''hidden variable,'' and in three dimensions at least, the exponents α, β, and γ are renormalized by division by $(1-\alpha)$. Since α is small, the change in the critical exponent is small, and in the present work, the error bars are too large to permit the observation of an effect.

As noted above, the data concerning the process of disordering of the $p4g$ structure to a $c(2\times2)$ structure is not

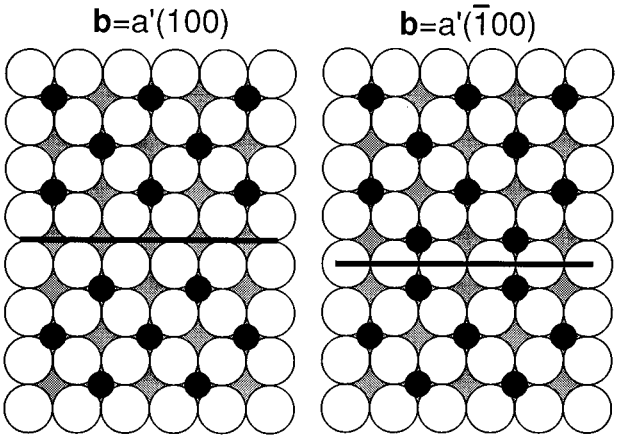

FIG. 8. Surface defects in the $c(2\times2)$ structure, with their respective surface Burgers vectors.

completely clear due to the proximity of the desorption temperature. However at $\Theta=0.5$, the $p4g$ can disorder to a $c(2\times2)$ by rotation of the motif of 4 Rh atoms and one oxygen atom. Mechanistically, this is unlikely to proceed via the creation of localized defects, as neighboring domains would interact strongly by Rh-Rh atom repulsion. Instead, the angle of rotation of each motif could go to zero continuously by vibrational excitation until the average angle is zero. If this is so, the angle of rotation would be identified with the spin parameter in magnetic terminology, and the appropriate model is the XY model, which has nonuniversal exponents.

V. CONCLUSIONS

The phase diagram of the O/Rh(100) system has been described semiquantitatively and the phase transitions from the $c(2\times2)$ and $p4g$ phases to disordered states have been characterized. The $(2\times2)p4g\rightarrow c(2\times2)$ transition has measured critical exponents which are consistent with the Ising model over all of the existence range of the $p4g$.

Emphasis has been placed on the microscopic mechanism for the transition. For example, at constant temperature and increasing coverage, the $p(2\times2)$ converts to the $c(2\times2)$ structure by the formation of extended defects which are heavy domain walls. Possible defects involved in the $c(2\times2)\rightarrow(1\times1)$ transition have been described. The nature of the $c(2\times2)$ phase has been investigated and is found to be nonstoichiometric and partly disordered over most of its existence range. The results have been interpreted in terms of adsorbate-adsorbate interaction, both for the kinetics of formation of the ordered phases and for the dynamics of disordering.

ACKNOWLEDGMENT

We thank Luca Gregoratti for help in the XPS measurements.

*Present address: IRC in Surface Science, University of Liverpool, Liverpool L69 3BX, U.K.

†Also at Dipartimento di Fisica, Università di Trieste, I-34127 Trieste, Italy.

[1] E. Kopatzki and R. J. Behm, Surf. Sci. **245**, 255 (1991).

[2] W. Oed, B. Dotsch, L. Hammer, K. Heinz, and K. Müller, Surf. Sci. **207**, 55 (1988).

[3] L. Gregoratti, A. Baraldi, G. Comelli, V. R. Dhanak, M. Kiskinova, and R. Rosei, Surf. Sci. **340**, 205 (1995).

[4] A. Baraldi, L. Gregoratti, G. Comelli, V. R. Dhanak, M. Kiskinova, and R. Rosei, Appl. Surf. Sci. **99**, 1 (1996).

[5] A. Baraldi, V. R. Dhanak, G. Comelli, K. C. Prince, and R. Rosei, Phys. Rev. B **53**, 4073 (1996).

[6] J. Mercer, P. Finetti, F. Leibsle, V. R. Dhanak, R. McGrath, A. Baraldi, K. C. Prince, and R. Rosei, Surf. Sci. **352**, 173 (1996).

[7] L. H. Dubois, J. Chem. Phys. **15**, 5228 (1982).

[8] C. W. Tucker, J. Appl. Phys. **37**, 3013 (1966).

[9] D. G. Castner, B. A. Sexton, and G. A. Somorjai, Surf. Sci. **71**, 519 (1978).

[10] G. C. Wang, T. M. Lu, and M. G. Lagally, J. Chem. Phys. **69**, 479 (1978).

[11] A. R. Kortan and R. L. Park, Phys. Rev. B **23**, 6340 (1981).

[12] D. E. Taylor and R. L. Park, Surf. Sci. **125**, L73 (1983).

[13] P. Piercy and H. Pfnür, Phys. Rev. Lett. **59**, 1124 (1987).

[14] K. De'Bell, H. Pfnür, and P. Piercy, ''*The Structure of Surfaces III*,'' Vol. 24, Springer Series in Surface Science (Springer-Verlag, Berlin, 1991).

[15] V. R. Dhanak, A. Baraldi, and K. C. Prince (unpublished).

[16] A. E. Ferdinand and M. E. Fisher, Phys. Rev. **185**, 832 (1969).

[17] D. P. Landau, Phys. Rev. B **13**, 2997 (1976).

[18] M. Zacchigna *et al.* (unpublished).

[19] K. Binder and D. P. Landau, Surf. Sci. **108**, 503 (1981).

[20] A. N. Salanov and V. I. Savchenko, Surf. Sci. **296**, 393 (1993).

[21] S. Reindl, A. A. Aligia, and K. H. Bennemann, Surf. Sci. **206**, 20 (1988).

[22] M. E. Fisher, Phys. Rev. **176**, 257 (1968).